

Using a structural genetic model to derive map distances and correlation

Chris Salahub
University of Waterloo

April 2, 2022

1 Introduction

Genetic research today routinely considers the entirety of a genome to identify the regions most strongly related to measured physical traits. The goal is to associate measured genome sequences, the *genotype*, with physical characteristics, the *phenotype*. Computational and methodological advances in the pursuit of these *quantitative trait loci* (QTLs) have distinguished *genomics* as its own field. Central to genomics is the *genome-wide association study* (GWAS), where many *markers*, sequences of nucleotides at known positions on the genome, are measured. Extracting useful results from markers and measured traits is a complicated task which has motivated decades of statistical and biological research. Interested individuals are left to sort through this research in order to understand genomics.



Figure 1: A structural model of a GWAS.

To aid in this, Figure 1 draws on the literature to present a simple structural model of the process taken in GWAS to convert raw marker measurements into a form which can be used to identify QTLs. It identifies four key steps (*selection*, *annotation*, *encoding*, and *summarization*) between five increasingly abstract representations of the genome, where the genome is defined by Doerge et al. (1997) as all heritable material potentially passed from parent to offspring. By highlighting the abstractions and steps in plain language, this simplified model provides a convenient map to guide the understanding of GWAS. This is not a replacement for surveys such as Uffelmann et al. (2021); Tam et al. (2019), instead it provides a guiding structural framework with exceptional explanatory power to facilitate understanding of other papers in the field.

The model starts with \mathbf{G} , the whole genome of an individual organism. Genetic information is stored in DNA, a long molecule consisting of a sequence of four *nucleotide bases*: guanine, cytosine, adenine, and thymine. A *diploidic* individual inherits one version or *variant* of a complete DNA sequence from each parent, and so has two copies in all *somatic* (i.e. non-reproductive) cells. Though it can be represented as one long sequence, DNA is actually structured into *chromosomes*, separate strands of DNA which contain only a part of the sequence. As most genetic research concerns diploidic species, this will be implicitly assumed.

It is usually not feasible or desirable to design a study around the measurement of all of \mathbf{G} , and so the *select* step chooses regions to measure. These regions are represented by \mathbf{S} . Often \mathbf{S} consists of a series of *single nucleotide polymorphisms* (SNPs), single nucleotide substitutions in a known sequence at a known position. In human studies this is supported by SNP databases such as NCBI (2021) which document hundreds of millions of common SNPs in the human genome. Only a small proportion of these are estimated to occur frequently enough in the population to be useful in a GWAS, perhaps 15 million according to Koboldt et al. (2013). Modern SNP arrays can simultaneously identify roughly one million of these per array, see LaFramboise (2009); Tam et al. (2019), and most GWAS will measure an array’s worth of SNPs. *Linkage disequilibrium*, effectively the correlation between regions of the genome, facilitates inference to regions outside of those selected in \mathbf{S} . While third generation genome sequencing technologies allow for entire genomes to be sequenced, as noted in Heather and Chain (2016); Hasin et al. (2017); Uffelmann et al. (2021), persistent high costs of next generation technologies and more than a decade of SNP microarray development leave microarrays as the dominant measurement method.

After selecting SNPs to obtain \mathbf{S} , researchers must *annotate* the raw data. The raw signal produced by an SNP microarray is fluorescence, with different degrees of fluorescence corresponding to a different genotypes. Converting the fluorescent areas of an array to a genotype is a challenging problem and has developed in tandem with the arrays themselves. Early models used non-parametric clustering techniques on the signal from several microarray pores, but more complex hidden Markov and Bayesian models have also been developed. LaFramboise (2009) details some of these. Whatever method is used, the selected regions are assigned genotypes in \mathbf{T} denoted with capital or lowercase letters at each SNP, as in Siegmund and Yakir (2007); Visscher and Goddard (2019).

Finally, relationships between \mathbf{T} and an observed trait or within \mathbf{T} itself are quantified by converting each annotated SNP to a number. To do this, GWAS first *encode* each SNP variant with a numeric value and then *summarize* the pairs at each location into a number. Typically no distinction is made between these steps: Lander and Botstein (1989); Cheverud (2001); Siegmund and Yakir (2007) detail the *dominance* and *additive* summaries by moving directly from a genotype to a numeric value. It is useful for clarity and full generality to separate the two distinct steps involved in this process, however.

This paper presents the details of this structural model. By using mathematical notation for each of the abstractions, a framework with extraordinary explanatory power is devised. Section 2 provides a detailed explanation of the model with all the necessary notation. The model is then used in a novel derivation of the Haldane *map distance*, a common measure used to locate SNPs, in Section 3. The utility of the model is further demonstrated in Section 4, where the model is used to derive the correlation between markers under classic breeding population settings. This results in a convenient expression of the correlation between markers in any genetic study. Finally, Section 6 compares the results of this derivation directly to experimental data in mice.

2 A structural genetic model

The structural model starts with

$$\mathbf{G} = [\mathbf{g}_1 | \mathbf{g}_2], \quad \mathbf{g}_1, \mathbf{g}_2 \in \mathcal{B}^{N_P}$$

where $\mathcal{B} = \{\text{adenine, guanine, cytosine, thymine}\}$ is the set of nucleotide bases and N_P is the length of the genome, in humans $N_P = 3,234,830,000$. \mathbf{G} represents the whole genome of an individual, with both the maternal and paternal variants of all chromosomes placed sequentially in adjacent columns. Both of these variants are complete, double-stranded sequences of DNA, but nucleotides pair uniquely. Adenine binds exclusively with thymine and guanine exclusively binds with cytosine. Therefore \mathbf{g}_1 and \mathbf{g}_2 record the pattern only for one of the two DNA strands for each column, the complementary strand being implied by this sequence.

Rather than address the whole genome, GWAS typically deal with a selected subset of segments on chromosomes of interest. This is represented by

$$\mathbf{S} = [\mathbf{s}_1 | \mathbf{s}_2], \quad \mathbf{s}_1, \mathbf{s}_2 \in \mathcal{B}^K$$

with $K \ll N_P$. This corresponds to a mapping from $\mathbf{G} \rightarrow \mathbf{S}$ where K rows of \mathbf{G} are chosen or sampled to create \mathbf{S} . These rows are not typically selected at random, but are motivated by previous work and databases of SNPs and other known markers. Most commonly, then, the mapping $\mathbf{G} \rightarrow \mathbf{S}$ is a selection of $M < K$ disjoint sequences from \mathbf{G} .

In the case of SNPs, the markers are most often *biallelic*, i.e. the population is dominated by two different sequences or *alleles* at the marker. These are often denoted using two different letters, such as A and B , or analogously the uppercase and lowercase version of the same letter, such as A and a . Converting the measured markers to letters is called annotation, which maps $\mathbf{S} \rightarrow \mathbf{T}$ with

$$\mathbf{T} = [\mathbf{t}_1 | \mathbf{t}_2], \quad \mathbf{t}_1, \mathbf{t}_2 \in \{A, a\}^M.$$

Denoting the i^{th} position of \mathbf{t}_j as t_{ij} , $t_{lj} = A$ and $t_{mj} = A$ do not represent identical sequences at positions l and m . Instead this indicates that the sequences annotated by the capital at each position are present at their respective positions.

These annotated variants in \mathbf{T} might next be converted to a numeric form. This is a mapping $\mathbf{T} \rightarrow \mathbf{X}$ such that

$$\mathbf{X} := [\mathbf{x}_1 | \mathbf{x}_2], \quad \mathbf{x}_1, \mathbf{x}_2 \in \mathbb{R}^M.$$

Commonly this is even more restricted with $\mathbf{x}_j \in \{0, 1\}^M$ where

$$x_{ij} = \begin{cases} 1, & \text{if } t_{ij} = A \\ 0, & \text{if } t_{ij} = a \end{cases}, \quad (1)$$

is an indicator of the presence of the allele denoted with a capital.

Finally, \mathbf{X} may be converted into a vector

$$\mathbf{z} \in \mathbb{R}^M$$

summarizing the individual's inherited variants. There are many common mappings $\mathbf{X} \rightarrow \mathbf{z}$. The *dominance mapping* takes $z_i = \max\{x_{i1}, x_{i2}\}$, the *homozygous mapping* uses $z_i = I_{x_{i2}}(x_{i1})$, and the *additive map* is $\mathbf{z} = \mathbf{x}_1 + \mathbf{x}_2$, where \mathbf{x}_1 and \mathbf{x}_2 are given according to Equation 1 and $I_y(x)$ is the indicator function

$$I_y(x) = \begin{cases} 1, & \text{if } x = y \\ 0, & \text{otherwise} \end{cases}.$$

The additive map gives $\mathbf{z} \in \{0, 1, 2\}^M$ so z_i is equal to the count of copies of A at the i^{th} marker across both of an individual's inherited variants.

Figure 1 displays this model, with descriptive names added to each mapping. In the first step, $\mathbf{G} \rightarrow \mathbf{S}$, we *select* segments of the entire genome to obtain the marker sequences of interest. The next step, $\mathbf{S} \rightarrow \mathbf{T}$, *annotates* the chosen markers by indicating which of the common alleles is present for that marker. These annotations are then converted to numeric values, or *encoded*, in the step $\mathbf{T} \rightarrow \mathbf{X}$. Finally, we *summarize* the matrix \mathbf{X} into a vector \mathbf{z} with some row-wise operation.

3 Deriving map distance

The structural model presented in Section 2 has incredible explanatory power beyond being a clear guide to GWAS data. With only a few assumptions, the model shows the Haldane map distance to be a corollary of the structure of DNA and mechanics of inheritance as understood today. This is in contrast to the typical derivation of map distance, which is based on a differential equation agnostic to the structure of genetic material, as in Kosambi (1943) and Xu (2013). The derivation of the Haldane map is outlined here. We begin with a simple sketch of sexual reproduction.

3.1 Sexual reproduction

Sexual reproduction is the recombination of the genome of two parents to create offspring genetic distinct from both. To discuss sexual reproduction, a distinction must be made between reproductive or *sex* cells, e.g. sperm, and non-reproductive or *somatic* cells. Sex cells contain only one variant of the genome, while somatic cells contain two.

Recall that there exist two variants of each chromosome within every somatic cell, a paternal variant and a maternal variant. Introduce two new matrices to represent the maternal and paternal genomes of which \mathbf{G} is the offspring:

$$\mathbf{M} = [\mathbf{m}_1 | \mathbf{m}_2] \text{ and } \mathbf{F} = [\mathbf{f}_1 | \mathbf{f}_2],$$

where $\mathbf{m}_1, \mathbf{m}_2, \mathbf{f}_1, \mathbf{f}_2 \in \mathcal{B}^{N_P}$. These represent the genomes of the parents of \mathbf{G} . Crudely, sexual reproduction is the construction of \mathbf{G} from one random column of \mathbf{M} and one random column of \mathbf{F} . So, \mathbf{G} could be $[\mathbf{m}_1 | \mathbf{f}_2]$, for example.

The real mechanism is much more complex. During meiosis, the production of sex cells, the columns of \mathbf{M} and \mathbf{F} are perturbed. Rather than being inherited by \mathbf{G} in the same form as in \mathbf{M} and \mathbf{F} , regions in \mathbf{f}_1 may swap with regions in \mathbf{f}_2 and the same may occur with \mathbf{m}_1 and \mathbf{m}_2 . This occurs either due to the *independent assortment of chromosomes* or due to the *crossing over* of variants.

Independent assortment is a direct consequence of the structure of the genome in somatic cells. Each chromosome is a separate molecule and so when sex cells are created, the parental variant inherited by offspring is independent of other chromosomes. This means that both the paternal and maternal variants of a chromosome are equally likely to be passed on regardless of the variant another chromosome passes on.

Additionally, these variants may not be inherited identically as they appear in \mathbf{M} or \mathbf{F} . There is a chance that the variants in a parent physically cross over each other while separating to form sex cells. Occasionally, this crossing results in a swap of the entire chromosome on either side of the cross, creating two completely new variants to pass on.

3.2 Modelling cross overs

Both crossing over and the independent assortment of chromosomes occur within each parental genome regardless of the genome of the other parent, and so only one of the two needs to be considered in modeling cross overs. Suppose it is \mathbf{M} .

We start with the assumption that genetic recombination is totally independent between chromosomes. Specifically, chromosomes not only assort independently but crossing over occurs independently on each chromosome and will affect only that chromosome's variants. This assumption can be thought of as a slightly stronger version of independent assortment. Therefore consider a vector

$$\mathbf{h} \in \{1, 2, \dots, C\}^{N_P}$$

for $C \in \mathbb{N}$ which denotes the chromosomal membership of each row of \mathbf{M} . Motivated by the structure of the genome, for all $i \leq j$ set $h_i \leq h_j$. In other words all base pairs of a chromosome appear in adjacent rows with some specified ordering of the chromosomes. Assuming cross overs occur independently for each chromosome, a cross over in chromosome c , say, will affect only those rows of \mathbf{M} where $\mathbf{h} = c$. For simplicity, then, consider the case where \mathbf{h} is a vector of ones, that is the case of a single chromosome. Any result derived for a single chromosome can then be extended to the entire genome by considering every other chromosome in the same way.

For this single chromosome, consider a cross over beginning at the i^{th} base pair. This means the two variants of the chromosome physically cross at the i^{th} base pair. Assume that the variants are always perfectly aligned so that the i^{th} position on one variant will match with the i^{th} on the other during a cross over. Each variant is consequently separated into two parts: the part up to, but not including, the i^{th} base pair, and the part from the i^{th} base pair until the end. These two parts are then swapped between the variants, so that the first part of one variant forms a new chromosome with the second part of the other. Whenever the verb "begin" is used in the context of the index of a cross over, it will refer to this sort of crossing: a swap of the values in the first $i - 1$ rows of \mathbf{M} . Introduce an indicator vector

$$\mathbf{v} = (v_1, \dots, v_{N_P})^T$$

where

$$V_i = \begin{cases} 1 & \text{if a cross over beginning at base pair } i \text{ occurs,} \\ 0 & \text{otherwise,} \end{cases} \quad (2)$$

and define π so that $\pi_i = P(V_i = 1)$. This can be done without loss of generality, as the order of crossing over events in time does not affect the final chromosome. Any chromosome in a sex cell for which any cross overs have occurred is called *recombinant*.

As we rarely sequence the entire genome of an individual's somatic and sex cells, we will seldom see \mathbf{M} and its recombinant forms. Instead, just as \mathbf{S} is derived from \mathbf{G} , \mathbf{M}_S and \mathbf{F}_S are derived from \mathbf{M} and \mathbf{F} respectively. Swaps of the markers of \mathbf{M}_S and \mathbf{F}_S appearing in \mathbf{S} are then used to estimate the number of sex cells containing recombinant chromosomes. The proportion of sex cells produced with such a swap is called the *recombination rate* for the pair of markers.

However, the recombination rate for a pair of markers tells us nothing of how many cross over events occurred between them. Any odd number of events leads to a swap, while any even number will be undetectable. With this restricted view, the true count of indices i for which $v_i = 1$ cannot be known, and hence the π_i cannot be estimated individually.

3.3 Simplifying assumptions

Fortunately, if the recombination of two particular markers on the genome is all we care about, estimating individual π_i values is unnecessary. Consider two such positions, j and k with $j < k$, and note that cross overs beginning at any of $j + 1, j + 2, \dots, k - 1, k$ all result in these positions being split between variants. For identifiability assume that $\pi_j = \pi_{j+1} = \dots = \pi_{k-1} = \pi_k = \pi_{j:k}$. Let N_c be a random variable counting the number of cross overs beginning in $\{j + 1, j + 2, \dots, k - 1, k\}$. Then

$$P(N_c = n_c) = \binom{k-j}{n_c} \pi_{j:k}^{n_c} (1 - \pi_{j:k})^{k-j-n_c}$$

if we assume the cross overs occur independently. For convenience, let $r = k - j$ and $\pi = \pi_{j:k}$, which gives

$$P(N_c = n_c) = \binom{r}{n_c} \pi^{n_c} (1 - \pi)^{r-n_c}, \quad (3)$$

where r is a unitless count of base pairs between positions j and k .

Recall that $N_P = 3,234,830,000$ in humans. This large number of base pairs spread over the 23 human chromosomes means that two markers will typically be separated by a great number of base pairs, and so r will be very large. Indeed, examples in [Nyholt \(2004\)](#), [Salyakina et al. \(2005\)](#), and [Galwey \(2009\)](#) typically have thousands or tens of thousands of base pairs between marker locations. Therefore, consider the limit of this expression as $r \rightarrow \infty$:

$$\lim_{r \rightarrow \infty} P(N_c = n_c) = \lim_{r \rightarrow \infty} \binom{r}{n_c} \pi^{n_c} (1 - \pi)^{r-n_c}.$$

At this point, a substitution can be made:

$$\pi = \frac{\beta d(j, k)}{r} := \frac{\beta d}{r},$$

with $\beta, d(j, k) \in \mathbb{R}$. This substitution reparametrizes the probability π with a rate parameter, β , a distance measure, $d(j, k)$, and the r base pairs separating j and k . As the units of β and d will always result in

a unitless product, the choices of β and d are a matter of individual discretion. Any distance d can be chosen and will invoke a corresponding β . If physical distance, for example in angstroms, were used, then β would correspond to a rate of cross overs per unit length. One could alternatively use $d(j, k) = k - j$ and use a rate per base pair. As such a substitution is arbitrary, it gives a great deal of flexibility to choose a convenient set of units for measurement or understanding.

The substitution also leads to a substantial simplification, as

$$\begin{aligned}
\lim_{r \rightarrow \infty} P(N_c = n_c) &= \lim_{r \rightarrow \infty} \frac{r(r-1) \dots (r-n_c)}{n_c!} \left(\frac{\beta d}{r} \right)^{n_c} \left(1 - \frac{\beta d}{r} \right)^{r-n_c} \\
&= \lim_{r \rightarrow \infty} \frac{r^{n_c} + O(r^{n_c-1})}{n_c!} \left(\frac{\beta d}{r} \right)^{n_c} \left(1 - \frac{\beta d}{r} \right)^{r-n_c} \\
&= \lim_{r \rightarrow \infty} \frac{r^{n_c} + O(r^{n_c-1})}{r^{n_c}} \left(\frac{(\beta d)^{n_c}}{n_c!} \right) \left(1 - \frac{\beta d}{r} \right)^{r-n_c} \\
&= \frac{(\beta d)^{n_c}}{n_c!} \lim_{r \rightarrow \infty} \frac{r^{n_c} + O(r^{n_c-1})}{r^{n_c}} \left(1 - \frac{\beta d}{r} \right)^{r-n_c} \\
&= \frac{(\beta d)^{n_c}}{n_c!} e^{-\beta d},
\end{aligned} \tag{4}$$

which is the Poisson limit theorem for the binomial distribution.

Recall that if N_c is odd, it will result in a swap of markers j and k between variants, while if N_c is even, there will be no swap in the chromosome passed on. Define the recombination probability $p_r(d)$, which gives the probability of observing a swap for positions j and k with distance $d(j, k) := d$ between them. Then $p_r(d)$ is given by a sum of all odd terms from Equation 3. Taking the simplification of Equation 4 gives

$$\begin{aligned}
p_r(d) &= \sum_{l=0}^{\infty} \frac{(\beta d)^{2l+1}}{(2l+1)!} e^{-\beta d} \\
&= e^{-\beta d} \sum_{l=0}^{\infty} \frac{(\beta d)^{2l+1}}{(2l+1)!} \\
&= e^{-\beta d} \left(\frac{e^{\beta d} - e^{-\beta d}}{2} \right) \\
&= \frac{1}{2} (1 - e^{-2\beta d}).
\end{aligned} \tag{5}$$

A final substitution converts Equation 5 to a form familiar to researchers in genomics. Setting $\beta = \frac{1}{100}$ so that each unit increase in d corresponds to a 0.01 increase in the expected number of crossing over events gives us Haldane’s formula for the *map distance* in *centiMorgans* or cM. By accounting for the structure of the genome and making a number of simplifying assumptions, the model from Section 2 gives a classic result of genetics without any reference to the population-level differential equation used in its original derivation. This comforting result can be taken a step further to compute new theoretical results.

4 Genetic correlation

Cheverud (2001); Li and Ji (2005); Galwey (2009) all present results based on the *correlation between markers*. Recall \mathbf{z} as depicted in Figure 1 and described in the beginning of Section 1. For these papers, the *correlation between markers* refers to the observed correlation matrix of the vector \mathbf{z} in a particular population. While the motivation of these authors is adjustment for multiple dependent testing, the importance of correlation in defining linkage disequilibrium makes the correlation structure of the genome a matter of general interest. Using the model of Section 2 and results of Section 3 this matrix can be determined analytically.

For clarity, let \mathbf{z} indicate an instance of the random vector $\mathbf{Z} = (Z_1, Z_2, \dots, Z_M)^\top$. We let the random vector \mathbf{Z} follow the distribution of the summarized values \mathbf{z} in a particular population. This population may be real, as is the case when this modelling is used in practice, or purely hypothetical, as will be the case in the following analysis.

Return to the annotated matrix \mathbf{T} and consider two markers at row indices j and k . Introduce \mathbf{c} , which is defined similarly to \mathbf{h} earlier, but now indicates chromosomal membership for the markers in \mathbf{T} rather than the base pairs in \mathbf{G} . As every marker is contained within a single chromosome, \mathbf{c} is always unambiguously defined.

There are two cases. Either j and k are on the same chromosome, that is $c_j = c_k$, or they are not, and so $c_j \neq c_k$. If these markers are not on the same chromosome, the assumptions of Section 3.2 dictate that there will be no correlation between Z_j and Z_k , as these markers will assort independently alongside their respective chromosomes. If they are on the same chromosome, let $d(j, k) = d$ be the distance between them measured in cM in Equation 5. Denote the dominant and recessive alleles with A and a respectively for j and use B and b analogously for k . Assume that the pairwise association of these markers in the population is of interest, i.e. that we can ignore all other markers on this chromosome in our analysis. Under this setting, we may consider a radically simplified \mathbf{T} , with 2 rows rather than M and taking the form

$$\mathbf{T} = \begin{bmatrix} A & a \\ b & B \end{bmatrix},$$

where the letters placed above are merely demonstrative. A simplified version of \mathbf{X} follows immediately from this \mathbf{T} . Consider

$$\mathbf{X} = \begin{bmatrix} x_{j1} & x_{j2} \\ x_{k1} & x_{k2} \end{bmatrix},$$

with all entries in $\{0, 1\}$. As was the case for \mathbf{z} , we can treat these lowercase entries as realizations of random variables X_{rs} , $r \in \{j, k\}, s \in \{1, 2\}$. Consider $Cor(Z_j, Z_k)$ for the population resulting from an

arbitrary cross of two parents. Then \mathbf{X} implies a \mathbf{Z} of

$$\mathbf{Z} = \begin{bmatrix} Z_j \\ Z_k \end{bmatrix} = \begin{bmatrix} X_{j1} + X_{j2} \\ X_{k1} + X_{k2} \end{bmatrix}.$$

The mechanics of sexual reproduction outlined in Section 3.1 and the genotype of the parents crossed to create \mathbf{X} determine the distribution of Z_j and Z_k . Recall \mathbf{M} and \mathbf{F} introduced alongside sexual reproduction. Introduce simplified, annotated forms of these matrices here to represent the paternal and maternal encodings

$$\mathbf{F}_X = \begin{bmatrix} f_{j1} & f_{j2} \\ f_{k1} & f_{k2} \end{bmatrix}, \text{ and } \mathbf{M}_X = \begin{bmatrix} m_{j1} & m_{j2} \\ m_{k1} & m_{k2} \end{bmatrix},$$

where all entries are once again in $\{0, 1\}$. Begin by assuming that \mathbf{F}_X and \mathbf{M}_X are known constants. There are theoretical populatins where this is true such as the F_2 intercross, where $f_{11} = m_{11} = f_{21} = m_{21} = 1$ and $f_{12} = m_{12} = f_{22} = m_{22} = 0$. Further assume that the variation in \mathbf{Z} results purely from the recombination by crossing over and independent assortment.

Begin with the expectation of \mathbf{Z} . Assuming no preferential inheritance of either variant, X_{j1} is equally likely to be either f_{j1} or f_{j2} and so takes a uniform distribution over these two possibilities. A similar logic for all other entries in \mathbf{X} applies, and so

$$\begin{aligned} E[\mathbf{Z}] &= \begin{bmatrix} E[X_{j1}] + E[X_{j2}] \\ E[X_{k1}] + E[X_{k2}] \end{bmatrix} \\ &= \frac{1}{2} \begin{bmatrix} f_{j1} + f_{j2} + m_{j1} + m_{j2} \\ f_{k1} + f_{k2} + m_{k1} + m_{k2} \end{bmatrix}, \end{aligned}$$

from which it follows

$$\begin{aligned} \text{Var}(Z_j) &= E[(X_{j1} + X_{j2})^2] - E[Z_j]^2 \\ &= \frac{1}{4} [(f_{j1} + m_{j1})^2 + (f_{j2} + m_{j1})^2 + (f_{j1} + m_{j2})^2 + (f_{j2} + m_{j2})^2] \\ &\quad - \frac{1}{4} (f_{j1} + f_{j2} + m_{j1} + m_{j2})^2. \end{aligned}$$

This can be simplified to give

$$\text{Var}(Z_j) = \frac{1}{4} [(f_{j1} - f_{j2})^2 + (m_{j1} - m_{j2})^2]. \quad (6)$$

Analogously,

$$\text{Var}(Z_k) = \frac{1}{4} [(f_{k1} - f_{k2})^2 + (m_{k1} - m_{k2})^2]. \quad (7)$$

Considering the covariance:

$$\begin{aligned} \text{Cov}(Z_j, Z_k) &= \text{Cov}(X_{j1} + X_{j2}, X_{k1} + X_{k2}) \\ &= \text{Cov}(X_{j1}, X_{k1}) + \text{Cov}(X_{j1}, X_{k2}) + \text{Cov}(X_{j2}, X_{k1}) + \text{Cov}(X_{j2}, X_{k2}). \end{aligned} \quad (8)$$

So the covariance is re-expressed as a sum of four terms, each of which can be considered in turn.

This can be further simplified by considering $Cov(X_{j1}, X_{k2})$ and $Cov(X_{j2}, X_{k1})$. Both of these terms measure the covariance between values on the diagonals of \mathbf{X} , that is the covariance between the maternally and paternally donated variants of the genome inherited from \mathbf{F}_X and \mathbf{M}_X , respectively. These covariances therefore measure the amount of *inbreeding* in a population, that is the degree to which parents tend to have the same genotype. In settings with unknown parents or when a population is being considered [Crow and Kimura \(1970\)](#) quantify these covariances with the coefficient r . With known parents, as in our case, these diagonal values are independent of each other and therefore uncorrelated. This can be confirmed by tedious algebra. Explicitly, $Cov(X_{j1}, X_{k2}) = Cov(X_{j2}, X_{k1}) = 0$.

The second pair of terms, $Cov(X_{j1}, X_{k1})$ and $Cov(X_{j2}, X_{k2})$, measure the covariance of encodings on the same variant, and so cannot be so easily dismissed. Instead, consider $Cov(X_{j1}, X_{k1})$ and expand:

$$Cov(X_{j1}, X_{k1}) = E[X_{j1}X_{k1}] - E[X_{j1}]E[X_{k1}].$$

The equal probability of inheritance of variants gives $E[X_{j1}] = \frac{1}{2}(f_{j1} + f_{j2})$ and $E[X_{k1}] = \frac{1}{2}(f_{k1} + f_{k2})$. Next consider $E[X_{j1}X_{k1}]$.

There are four possible values of $X_{j1}X_{k1}$, corresponding to inheritance of either of the two parental variants with or without recombination. If no recombination occurs, an event with probability $1 - p_r(d)$, either $f_{j1}f_{k1}$ or $f_{j2}f_{k2}$ is inherited with equal probability. If a cross over between j and k leads to recombination, then either $f_{j1}f_{k2}$ or $f_{j2}f_{k1}$ is passed on with equal probability. Accounting for these four possibilities gives

$$E[X_{j1}X_{k1}] = (1 - p_r(d)) \left(\frac{1}{2}f_{j1}f_{k1} + \frac{1}{2}f_{j2}f_{k2} \right) + p_r(d) \left(\frac{1}{2}f_{j1}f_{k2} + \frac{1}{2}f_{j2}f_{k1} \right).$$

Combining this with the expectations of X_{j1} and X_{k1} gives

$$\begin{aligned} Cov(X_{j1}, X_{k1}) &= E[X_{j1}X_{k1}] - E[X_{j1}]E[X_{k1}] \\ &= (1 - p_r(d)) \left(\frac{1}{2}f_{j1}f_{k1} + \frac{1}{2}f_{j2}f_{k2} \right) + p_r(d) \left(\frac{1}{2}f_{j2}f_{k1} + \frac{1}{2}f_{j1}f_{k2} \right) \\ &\quad - \frac{1}{4}(f_{j1} + f_{j2})(f_{k1} + f_{k2}) \\ &= \frac{1}{4}(1 - 2p_r(d))(f_{j1}f_{k1} + f_{j2}f_{k2} - f_{j2}f_{k1} - f_{j1}f_{k2}) \\ &= \frac{1}{4}(1 - 2p_r(d))(f_{j1} - f_{j2})(f_{k1} - f_{k2}). \end{aligned} \tag{9}$$

The same logic can be applied to $Cov(X_{j2}, X_{k2})$ to obtain

$$Cov(X_{j2}, X_{k2}) = \frac{1}{4}(1 - 2p_r(d))(m_{j1} - m_{j2})(m_{k1} - m_{k2}). \tag{10}$$

We obtain the covariance of Z_j and Z_k by adding the above and Equation 8. Substituting Equations 9 and 10 and $Cov(X_{j1}, X_{k2}) = Cov(X_{j2}, X_{k1}) = 0$ gives

$$Cov(Z_j, Z_k) = \frac{1}{4}(1 - 2p_r(d)) [(f_{j1} - f_{j2})(f_{k1} - f_{k2}) + (m_{j1} - m_{j2})(m_{k1} - m_{k2})]. \quad (11)$$

Finally, Equations 6, 7, and 11 can be combined to determine the correlation:

$$\begin{aligned} Corr(Z_j, Z_k) &= \frac{Cov(Z_j, Z_k)}{\sqrt{Var(Z_j)Var(Z_k)}} \\ &= \frac{\frac{1}{4}(1 - 2p_r(d)) [(f_{j1} - f_{j2})(f_{k1} - f_{k2}) + (m_{j1} - m_{j2})(m_{k1} - m_{k2})]}{\frac{1}{4}\sqrt{[(f_{j1} - f_{j2})^2 + (m_{j1} - m_{j2})^2][(f_{k1} - f_{k2})^2 + (m_{k1} - m_{k2})^2]}} \\ &= (1 - 2p_r(d)) \frac{(f_{j1} - f_{j2})(f_{k1} - f_{k2}) + (m_{j1} - m_{j2})(m_{k1} - m_{k2})}{\sqrt{[(f_{j1} - f_{j2})^2 + (m_{j1} - m_{j2})^2][(f_{k1} - f_{k2})^2 + (m_{k1} - m_{k2})^2]}} \\ &:= (1 - 2p_r(d))\gamma. \end{aligned} \quad (12)$$

So, the correlation is a product of $(1 - 2p_r(d))$, which depends on the markers in question, and a factor γ , which depends on the parents being crossed. An even simpler expression is obtained by substituting the Haldane recombination probability from Equation 5 in place of $p_r(d)$:

$$\begin{aligned} Corr(Z_j, Z_k) &= (1 - 2p_r(d))\gamma \\ &= \left(1 - 2 \left[\frac{1}{2} (1 - e^{-2\beta d}) \right] \right) \gamma \\ &= \gamma e^{-2\beta d}, \end{aligned} \quad (13)$$

and so using the Haldane map distance the correlation between Z_j and Z_k decays exponentially in $d(j, k)$ with an intercept γ determined by the parents being crossed. Noted that as $f_{rs}, m_{rs} \in \{0, 1\}$, the differences defining γ are all either -1, 0, or 1. There are therefore $3^4 = 81$ potential γ values, though most of these are not unique. Indeed, across all 81 combinations

$$\gamma \in \left\{ -1, -\frac{1}{\sqrt{2}}, 0, \frac{1}{\sqrt{2}}, 1 \right\}.$$

A number of population settings for γ are of particular interest due to their use throughout history in mouse breeding experiments.

The first of these is the the F_2 *intercross* design. *Cross* here is short for sexual reproduction, not crossing over. This design considers the population resulting from the cross of \mathbf{M}_X and \mathbf{F}_X with

$$\mathbf{F}_X = \mathbf{M}_X = \begin{bmatrix} 1 & 0 \\ 1 & 0 \end{bmatrix}.$$

This corresponds to a setting where all the differences in γ are 1 and so $\gamma_{\text{inter}} = 1$.

The next is the F_2 *backcross*. Here we have a cross between \mathbf{M}_X and \mathbf{F}_X defined as

$$\mathbf{F}_X = \begin{bmatrix} f & f \\ f & f \end{bmatrix}, \text{ and } \mathbf{M}_X = \begin{bmatrix} 1 & 0 \\ 1 & 0 \end{bmatrix}.$$

where $f \in \{0, 1\}$. In this setting, both differences defined on \mathbf{F}_X are 0 while both of those defined on \mathbf{M}_X are 1. This gives $\gamma_{\text{back}} = 1$, the same as that of the intercross population.

Other interesting cases without historical names involve

$$\mathbf{F}_X = \begin{bmatrix} 0 & 1 \\ 1 & 0 \end{bmatrix} \text{ or } \mathbf{M}_X = \begin{bmatrix} 0 & 1 \\ 1 & 0 \end{bmatrix},$$

as these can result in $\gamma < 0$, and so a negative correlation. For example, if we have

$$\mathbf{F}_X = \mathbf{M}_X = \begin{bmatrix} 0 & 1 \\ 1 & 0 \end{bmatrix},$$

then $\gamma = -1$, while taking

$$\mathbf{F}_X = \begin{bmatrix} 0 & 1 \\ 1 & 0 \end{bmatrix} \text{ and } \mathbf{M}_X = \begin{bmatrix} 0 & 1 \\ 0 & 1 \end{bmatrix},$$

gives $\gamma = -\frac{1}{\sqrt{2}}$. Many other settings lead to no measured correlation. Take

$$\mathbf{F}_X = \begin{bmatrix} 0 & 1 \\ 1 & 0 \end{bmatrix} \text{ and } \mathbf{M}_X = \begin{bmatrix} 1 & 1 \\ 0 & 0 \end{bmatrix},$$

or

$$\mathbf{F}_X = \begin{bmatrix} 0 & 1 \\ 1 & 0 \end{bmatrix} \text{ and } \mathbf{M}_X = \begin{bmatrix} 1 & 1 \\ 0 & 0 \end{bmatrix},$$

for example.

Finally, these results can be extended to the whole genome. Recalling that j and k were restricted to be markers on the same chromosome, this pairwise result can be generalized to the correlation matrix of \mathbf{Z} for the markers measured on an entire genome. For markers on the same chromosome, non-trivial correlations will be proportional to $1 - 2p_r(d)$, where $p_r(d)$ is the probability of recombination as a function of the distance between markers. Based on the independent assortment of different chromosomes, the correlations will be zero for any pair j and k not on the same chromosome.

In other words, if $c_j = c_k$, Equation 12 dictates the correlation between Z_j and Z_k . On the other hand, if $c_j \neq c_k$ the correlation between Z_j and Z_k will be zero. This implies a block diagonal structure corresponding to the chromosomes with correlations dictated by the probability of recombination within each chromosome. Most generally

$$\text{Corr}(Z_j, Z_k) = I_{\{c_j\}}(c_k) \gamma(1 - 2p_r(d)), \quad (14)$$

and under the Haldane model Equation 13 gives

$$\text{Corr}(Z_j, Z_k) = I_{\{c_j\}}(c_k) \gamma e^{-2\beta d(j,k)}. \quad (15)$$

5 Simulating the model

The correlation results of Equation 15 are simulated by combining the model in Section 2 with the map distance derivation of Equation 5. A structure which mirrors \mathbf{T} is first created. It consists of two columns of annotated biallelic markers. These may be on separate chromosomes with intra-chromosome distances specified together with a function to generate recombination probabilities given a distance. By default, these distances and probabilities are cM and Equation 5. A population can be generated from a pair of these matrices with genetic recombination dictated only by independent assortment and crossing over, with the details matching those in Section 2. Each individual genome generated can then be encoded and summarized before the population-wide correlation matrix is computed.

Previous literature motivates particular simulation settings. [Cheverud \(2001\)](#) investigates the correlation matrix by simulating a single chromosome with equidistant markers. All combinations of chromosome lengths of 50, 75, and 100 cM with markers equidistant at 50, 25, 12.5, and 6.25 cM were simulated for populations of 500 F_2 intercross offspring. [Lander and Botstein \(1989\)](#) instead simulates twelve chromosomes of length 100 cM with markers every 20 cM along each for a population of 250 F_2 backcross offspring.

Departing from a reference to distances in cM or base pairs, [Li and Ji \(2005\)](#) set their simulation scenarios using the genetic r^2 measure as defined in [Hill and Robertson \(1968\)](#). This measure is exactly Pearson’s product moment correlation for the two by two contingency table case. This difference is meaningful, as [Siegmund and Yakir \(2007\)](#) note that r^2 is not constant over generations. After k generations it is given by

$$r_k^2 = [1 - p_r]^{2k} r_0^2$$

for two markers with $r^2 = r_0^2$ initially and a probability of recombination of p_r . Unlike cM or base pairs, which are constant over generations, r^2 eventually goes to zero.

Nonetheless, [Li and Ji \(2005\)](#) simulate 10 independent regions within each of which 5 markers are placed such that adjacent markers have an r^2 of 0.8 between them. This design is analogous to that of [Lander and Botstein \(1989\)](#), despite the difference in description.

Some of the simulations of [Cheverud \(2001\)](#) and [Lander and Botstein \(1989\)](#) were recreated using the implementation detailed above. Specifically, these were the 100 cM chromosome with 6.25 cM separated markers of [Cheverud \(2001\)](#) and the twelve 100 cM chromosomes with 20 cM separated markers of [Lander and Botstein \(1989\)](#). The resulting correlation matrices and theoretical correlation matrices are visualized side by side using heatmaps in Figures 2 and 3. In each heat map, the position of a square corresponds to the position of the corresponding correlation in the correlation matrix, and darker squares have a larger magnitude of correlation than lighter squares. Blue squares indicate negative correlation while red squares indicate a positive correlation.

Figure 2(a) displays a pattern of constant off-diagonal lines of decreasing value, as expected from Equation 5. Roughly the same pattern is seen in Figure 2(b), though it is much noisier. Rather than having clear constant lines along each off-diagonal, Figure 2(b) has regions of similar values which occur across several off-diagonal lines. This leads to the appearance of large squares of more strongly related values, a pattern absent from Figure 2(a).

Figure 3 displays the [Lander and Botstein \(1989\)](#) setting with the addition of guide lines to aid in reading the plot. These guide lines extend from labels on the top and left sides of the plot to indicate the chromosome of each marker. These lines create square borders along the diagonal which distinguish

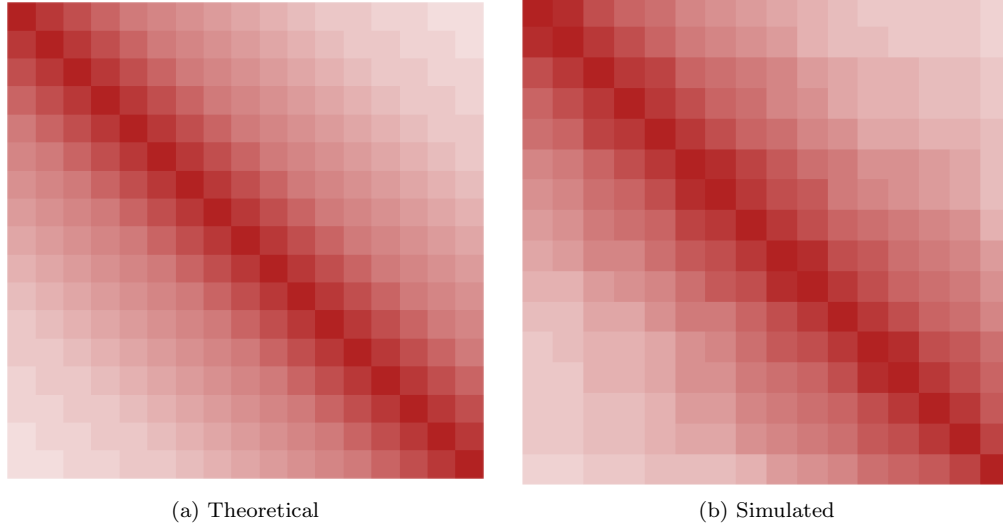


Figure 2: The correlation matrices of a population of 500 F_2 intercross offspring measured on a 100 cM chromosome with markers each 6.25 cM apart.

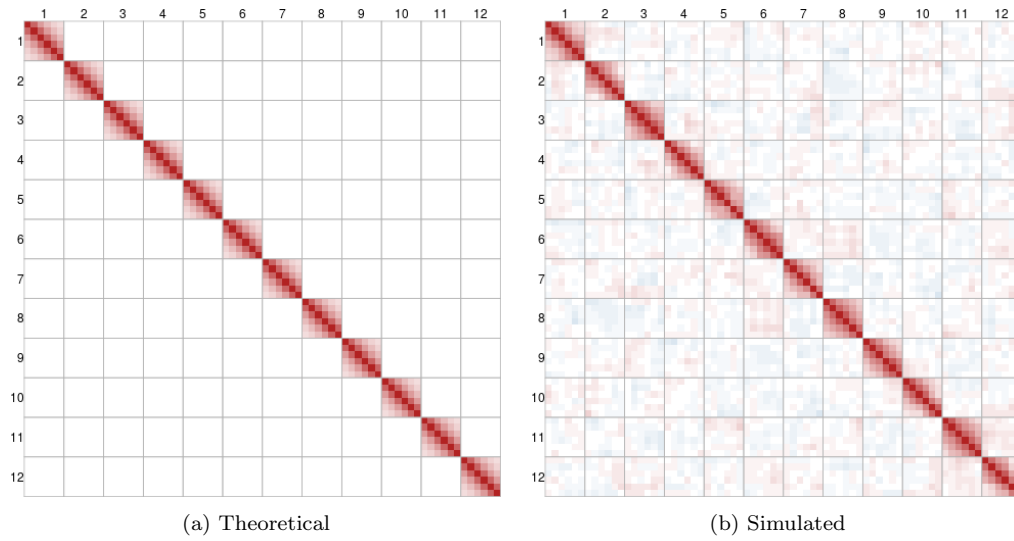


Figure 3: The correlation matrices of a population of 250 F_2 backcross offspring measured on twelve 100 cM chromosomes with markers 20 cM apart on each.

the intra-chromosome correlations within their borders from the inter-chromosome correlations outside of them. As suggested by Equation 5 and shown in Figure 3(a), Figure 3(b) has a stark block diagonal structure which agrees with these dark borders. The simulation therefore agrees very well with theory in this aspect. Within the chromosomes, there is also good agreement between Figure 3(a) and Figure 3(b). Both have decreasing correlations along the off-diagonal lines, with Figure 3(b) displaying similar departures from Figure 3(a) as Figure 2(b) does from Figure 2(a).

A more interesting noise pattern is seen between chromosomes outside the darker borders in Figure 3(b). Unlike the strictly positive correlations seen in Figure 2, both negative and positive correlations are observed. Though many chromosomes show consistent patterns between their markers, with all correlations either positive or negative as between chromosomes 9 and 6 or 11 and 12, many have more complicated relationships. Between chromosomes 7 and 3, for example, both negative and positive correlations are observed between markers which are larger than the smallest intra-chromosomal correlations within 2.

6 Comparing the model to reality

Though simulation confirms that population correlations generated under the model of Section 2 match the predictions of Equation 15, this does not mean it reflects genetic mechanics with fidelity. Evaluating the extent to which this is the case requires data. As Lander and Botstein (1989) and Cheverud (2001) only perform simulations, other sources are required.

The Mouse Genome Database (MGD) of Bult et al. (2019) provides annotation data for more than a dozen mouse populations resulting from crosses of known strains, alongside the references needed to determine cM distances between markers measured in these experiments. All of these resources are publicly provided at the Mouse Genome Informatics website: www.informatics.jax.org.

Considering only those experiments with complete observations leaves several data sets. Two of these investigate an identical population setting: the *BSB mouse cross* of Fidler et al. (1993). BSB mice are those resulting from the F_2 backcross of the C57BL/6J and *Mus Spretus* mouse strains, detailed respectively in JAX (2022) and Dejager et al. (2009). The first of these crosses is the *JAX BSB* cross of Rowe et al. (1994) and the second is the *UCLA BSB* cross of Welch et al. (1996). Both were downloaded from <http://www.informatics.jax.org/downloads/reports/index.html>.

The data sets require further cleaning before being used, however. First, any markers which do not have a known position along a chromosome in cMs are removed for both data sets. Following that, any individual mice with incomplete data are excluded. For the JAX BSB data this leaves 94 mice annotated at 1496 markers while the UCLA BSB data has 66 mice annotated at 111 markers. The correlation matrices for these data sets are displayed in Figures 4(a) and 5(a) respectively.

The cM positions of these markers were used to simulate 10,000 crosses under each of the JAX BSB and UCLA BSB settings using the methods of Section 5. Figures 4(b) and 5(b) display example correlation matrices from one such simulated population. For each setting, the quantile of the each experimental pairwise correlation was then computed using the 10,000 simulated crosses. Figures 4(c) and 5(c) display those quantiles which are less than 250 in blue and those which are greater than 9,750 in red for their respective settings. These correspond to unadjusted 95% confidence rejection regions for each correlation.

Qualitatively, the simulated examples show good agreement to experimental results. In both Figures 4 and 5 the patterns of correlation between chromosomes are similar between experiment and simulation

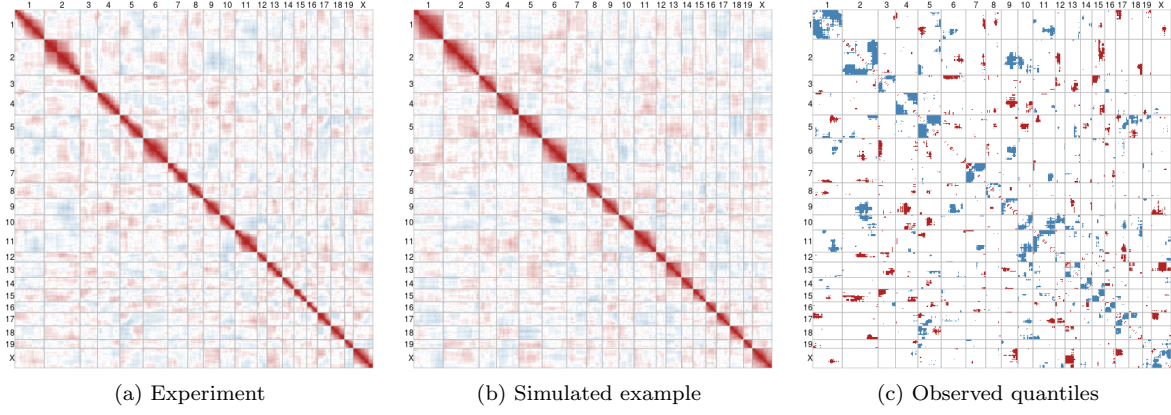


Figure 4: Observed and simulated correlations for the [MGD JAX BSB cross](#) from [Rowe et al. \(1994\)](#). (c) displays quantiles determined from 10,000 simulated crosses, those quantiles less than 250 are shaded blue and those greater than 9,750 are shaded red.

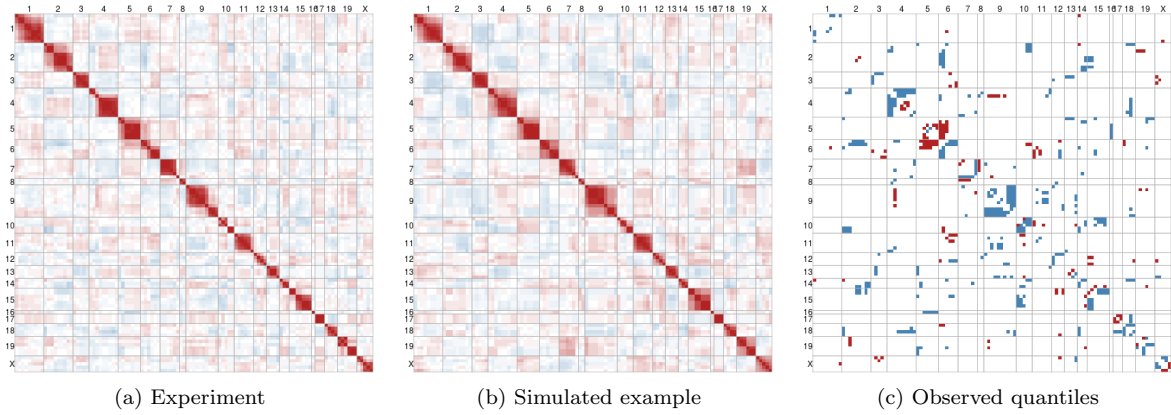


Figure 5: Observed and simulated correlations for the [MGD UCLA BSB cross](#) from [Welch et al. \(1996\)](#). (c) displays quantiles determined from 10,000 simulated crosses, those quantiles less than 250 are shaded blue and those greater than 9,750 are shaded red.

of the model from Section 2. Figures 4(c) and 5(c) additionally suggest that these patterns are little more than noise. The regions of unusually strong correlations shaded in red do not appear to follow any clear pattern, nor do the patterns of unusually weak correlations shaded in blue.

The similarity continues within chromosomes. Figures 4(c) and 5(c) are generally not shaded within chromosomes. in particular close to the diagonal. The most noteworthy pattern in either occurs in the corners of the diagonal squares corresponding to chromosomes in Figure 4(c). Many of these corners are shaded blue, suggesting these distant intra-chromosome correlations are less than might be expected in the JAX BSB cross for many chromosomes. The pattern of shading is suggestive of block structures within chromosomes where contiguous sections are fit well by the model but may have more complex dynamics between them.

A likely culprit is the assumption of independent cross overs. [Broman et al. \(2002\)](#) evaluated the pattern of cross overs in the [Rowe et al. \(1994\)](#) experiment, the basis of the JAX BSB data. Their results suggest that there is some *interference* between cross overs, that they are not fully independent. Most mouse chromosomes are much less than 100 cM in length, yet cross overs rarely occur within 20 cM of each other and fewer cross overs than expected occur on the same chromosome in a single meiosis event. This interference will have little impact on the correlation between markers with short distances between them, as more than one cross over event is unlikely to occur in a short interval. Markers separated by longer distances are impacted by this observed interference to a greater extent, as the observed number of double cross overs will be less than expected. This increases chance that distant markers will be separated in meiosis by a single crossover, leading to a weaker correlation than predicted.

That said, it is important not to over-interpret this pattern. It is not repeated in Figure 5 and the shading of quantile has not been adjusted to account for the many multiple tests performed in each plot. In order to get a greater sense of this experimental departure from theory, the common markers measured between the UCLA BSB and JAX BSB data were identified and the correlation matrices computed for these common locations. By having two experimental replicates the impact of one unusual measurement is reduced. These correlations are displayed in Figure 6.

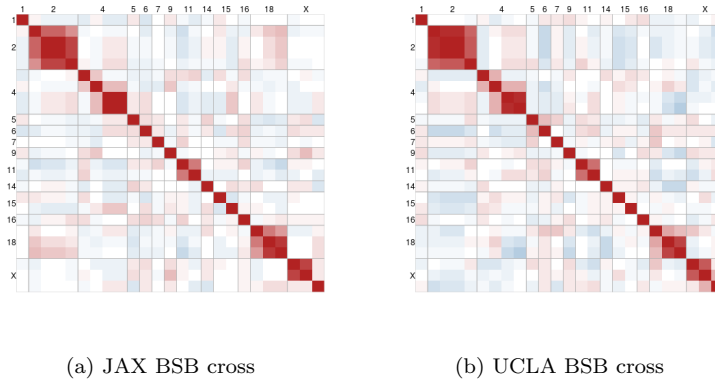


Figure 6: Observed pairwise correlations for the marker positions measured in both [Rowe et al. \(1994\)](#) and [Welch et al. \(1996\)](#).

Most chromosomes have only one marker measured in common between these experiments, but chromosomes 2, 4, and 18 have several. Of particular interest is chromosome 2, which has a very different pattern in Figure 6(a) than in Figure 6(b).

A more detailed exploration is given by simulation. The common markers on chromosomes 2 and 4 were used to generate 10,000 simulated crosses of 80 mice, the average of the JAX and UCLA BSB cross populations. For any pair of markers the resulting distributions can then be compared to the experimental results of Rowe et al. (1994) and Welch et al. (1996) using the two-by-two layouts of Figure 7.

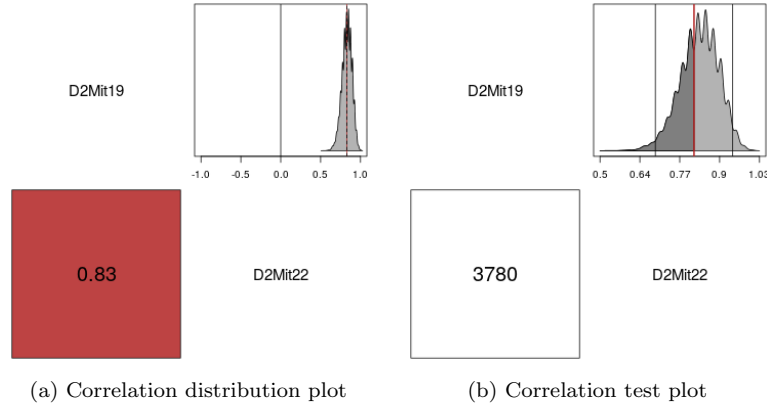


Figure 7: The correlation plots.

Each of the two subplots of Figure 7 consists of four cells. Along the diagonal, each cell provides one MGD marker symbol to display the pair of markers being compared. Above the diagonal a distribution is displayed, in both cases the kernel density estimate of the correlation over the 10,000 simulated crosses of 80 mice. Below the diagonal a numeric summary with some informative shading is displayed.

Figure 7(a) displays the kernel density estimate on a plot reflecting the range of possible correlations in the upper cell and the mean value of these correlations shaded with the divergent palette of Figures 2 to 6 in the lower cell. A solid black line at the theoretical value predicted by Equation 5 and dashed red line at the observed mean are also added to the upper cell. Figure 7(b) displays the kernel density estimate in more detail by placing the kernel density estimate in a plot with limits set by the estimate in the upper cell. Two solid lines are added at the correlations computed from the JAX and UCLA BSB data and a thicker red line is added at their mean, below which the density is shaded. The lower cell of Figure 7(b) communicates the quantile of this red line, or how many simulated correlations fall in the shaded region. As in Figures 5 and 4, this cell is shaded blue if the quantile is less than 250 and red if it is greater than 9,750.

For the two markers being compared in particular in Figure 7, D2Mit19 and D2Mit22, a number of aspects are of note. Figure 7 again demonstrates the close agreement of simulation and theory and communicates the spread of the markers. Across all simulations a relatively strong and positive correlation was observed which was always above 0.5. The lower panel provides the mean information at a glance in the same way as earlier correlation plots. Figure 7 compares the experimental results to this simulated distribution and finds good agreement between the simulated and experimental values. A more interesting

feature to note is the roughness of the kernel density estimate, which suggests a discrete distribution of correlations. Rather, it seems the population of 80 mice can have only certain values for the correlation between these markers in simulation.

By expanding the pairwise units of Figure 7 into larger arrays, the distributions of all pairwise correlations for the common markers on chromosomes 2 and 4 between the JAX and UCLA BSB crosses can be viewed. Along the diagonal, all eight marker symbols are displayed. For any cell, the corresponding pair of markers can be found by tracing along the row and column until the diagonal is reached. Interpretation then follows as in the two-by-two case. In an array, the entire pattern can also be seen at a glance, especially using the lower cells. This can then guide inspection of the upper panels. Such an expansion of Figure 7(a) gives the *correlation distribution plot* of Figure 8, while for Figure 7(b) the *correlation test plot* of Figure 9 results.

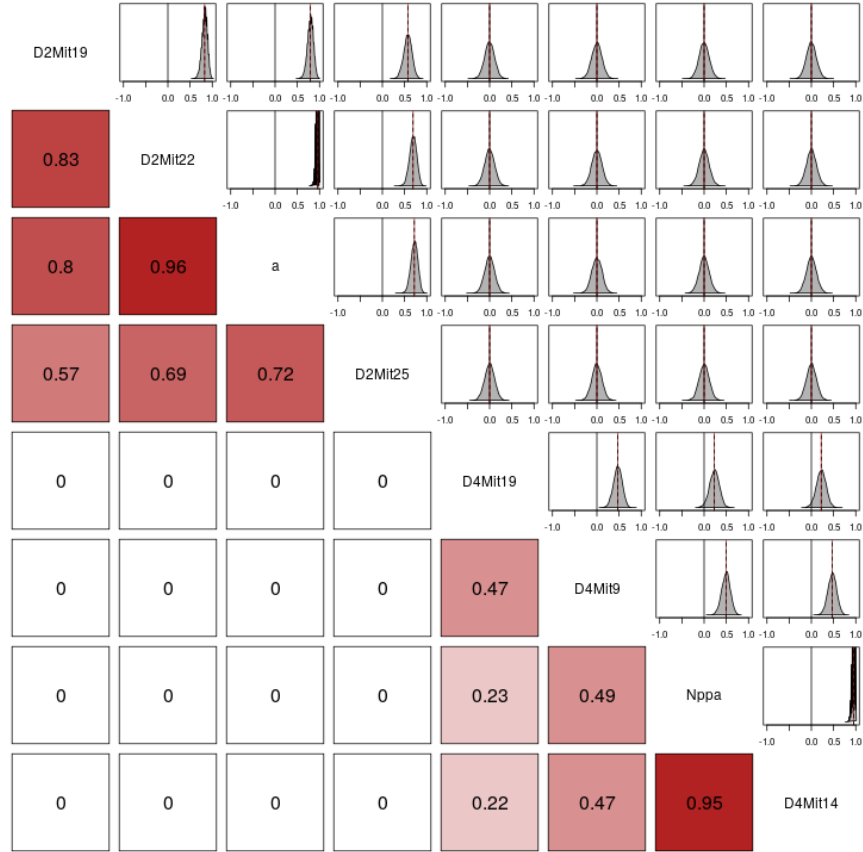


Figure 8: The *correlation distribution plot* for the common markers in the JAX and UCLA BSB cross experiments and their means over 10,000 simulated crosses.

The construction of Figure 8 is motivated by the correlation matrices seen in Figures 2 to 6. Indeed, the cells of the matrix of plots below the diagonal in Figure 8 reports the mean correlation across all simulated

crosses for the corresponding pair of markers given by the marker names along the diagonal. These cells are then shaded using the same divergent palette as earlier figures. It therefore serves as a more detailed version of lower part of the the earlier correlation heatmaps.

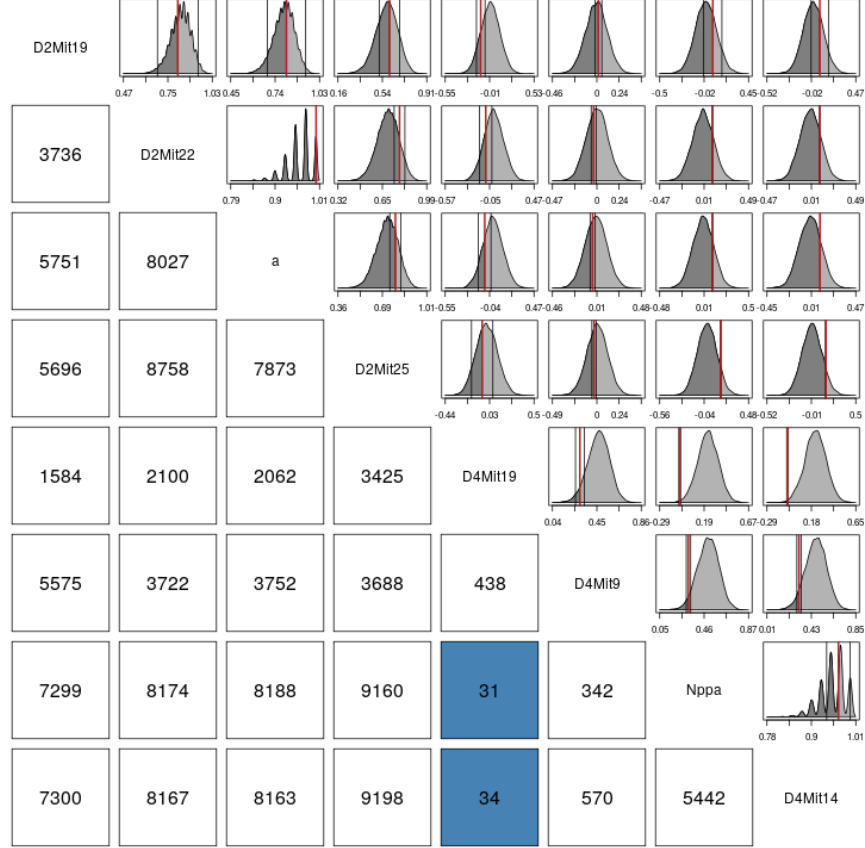


Figure 9: The correlation test plot for the JAX and UCLA BSB crosses. The upper cells show the distributions in detail with both crosses marked by black lines and their means marked by a red line, the bottom cells give the quantile of the corresponding mean over 10,000 simulated crosses.

The cells above the diagonal display kernel density estimates of the distribution of correlations across all 10,000 simulated crosses. Plotted over these are several lines. The first is a reference line at zero to add context to the density. A dashed red line indicates the theoretical correlation and a dashed black line indicates the mean correlation reported in the lower cells. In this way the correlation distribution plot provides information not only about the correlation structure of the data, but also about the variation expected under a simulation.

The distributions of the pairwise correlations are generally symmetric, unimodal and centred about the theoretical predictions. For markers close together with strong correlations between them, there appears to be some roughness to the density estimate, but for all others the densities appear smooth. The *correlation*

test plot of Figure 9 shows these densities in greater detail and displays the experimental results alongside the simulated distribution.

To see these densities in greater detail and how the experimental results compare, the plot bounds of the uppers cells can be set by each density, rather than globally. Lines for each experimental result and their mean can then be added. The lower cells can be made more informative by reporting the quantile of the mean and then shaded as in Figures 4(c) and 5(c) to display significant quantiles.

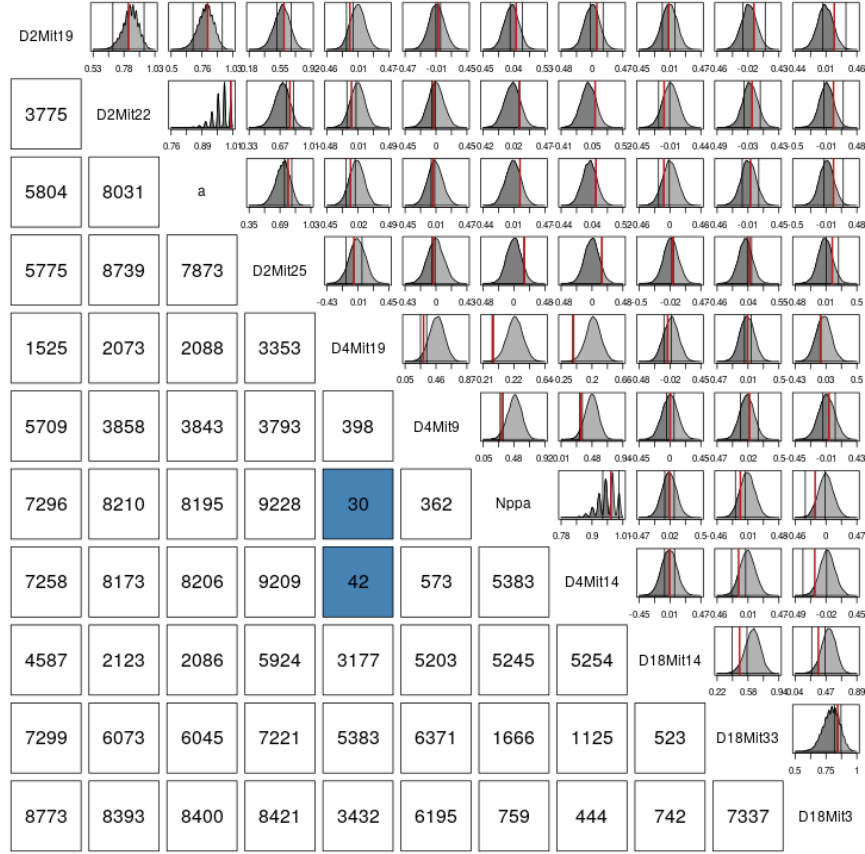


Figure 10: Adding chromosome 18's three common markers to Figure 9.

The most striking feature of both Figure 4(a) and Figure 5(a) is the block diagonal structure consistent with the independent assortment of chromosomes. The chromosomes form clear blocks with strong intra-chromosome correlations and weaker, noisier inter-chromosome correlations. Both of these data sets additionally show large correlations close to the diagonal and smaller correlations moving away from the diagonal within chromosomes. Between the chromosomes, an almost identical pattern of patches is observed in both. All of these patterns are mimicked by the simulation, showing prominently in Figures 4(b) and 5(b).

7 Conclusion

Despite this, many of the introductions to the field rely on the models of early pioneers of genetics. The works of Mendel, Pearson, Fisher, Haldane, and others in genetics were groundbreaking, but also occurred well before a modern understanding of DNA or the mechanics of inheritance [Visscher and Goddard \(2019\)](#). As a result, these models do not provide a modern context. Modern textbooks and papers consequently introduce the structure of DNA and the models describing inheritance in separate sections, if the structure of DNA is addressed at all [Crow and Kimura \(1970\)](#); [Siegmund and Yakir \(2007\)](#); [Xu \(2013\)](#); [Liu \(1998\)](#). Such complete and detailed accounts with the biology and statistics separated are unquestionably important, but fail to present an accessible and unified picture of genomics for researchers with a statistical background. **TODO: Move to conclusion: “this model provides a map to help understand larger works”**

[LaFramboise \(2009\)](#) notes that microarrays remove the middle steps entirely: by taking luminance directly it is possible to inspect and relate \mathbf{z} to physical characteristics without subjective intermediate steps.

This framework may not be limited to genomics. [Hasin et al. \(2017\)](#) note the expansion of genome-wide methods to protein and RNA sequencing. In both of these cases, the framework above applies, but has less explanatory power. One might imagine investigating proteins using this framework to see which are relatively under or over-expressed

Each of these italicized steps could be performed in a number of ways, with consequences on the final quantification of the genome’s relevant features. Selection typically involves the choice of at most one million SNPs from an SNP database such as [NCBI \(2021\)](#). Though these databases have hundreds of millions of identified SNPs, [Koboldt et al. \(2013\)](#) suggests that perhaps only 15 million are common enough to be useful, and that no further useful SNPs are likely to be found. While modern microarray technology dictates the limit on the number of simultaneously selected SNPs, see [LaFramboise \(2009\)](#); [Tam et al. \(2019\)](#), studies such as [Assimes et al. \(2016\)](#) often choose far fewer. These rely on SNPs used in previous literature and ready-made general microarrays as selection criteria. [Lander and Botstein \(1989\)](#) proposes SNPs selected uniformly across the genome for agnostic studies.

There are new technologies which allow entire genomes to be sequenced, see [Heather and Chain \(2016\)](#); [Hasin et al. \(2017\)](#); [Uffelmann et al. \(2021\)](#), but even when these reach a cost and speed accessible to most researchers there is little doubt known markers with previous literature will still be the focus of many studies. These technologies are more likely to expand the selection pool than to make selection irrelevant.

Categorical measures of association, such as the χ^2 test, could readily be applied to \mathbf{T} , where each possible row combination is treated as a different category. Such measurement would likely be more computationally inefficient, but would entirely circumvent the last two steps of Figure 1.

References

Themistocles L Assimes, I-T Lee, Jyh-Ming Juang, Xiuqing Guo, Tzung-Dau Wang, Eric T Kim, Wen-Jane Lee, Devin Absher, Yen-Feng Chiu, Chih-Cheng Hsu, et al. Genetics of coronary artery disease in taiwan: a cardiometabochip study by the taichi consortium. *PLoS One*, 11(3):e0138014, 2016.

- Karl W Broman, Lucy B Rowe, Gary A Churchill, and Ken Paigen. Crossover interference in the mouse. *Genetics*, 160(3):1123–1131, 2002.
- Carol J Bult, Judith A Blake, Cynthia L Smith, James A Kadin, Joel E Richardson, and the Mouse Genome Database Group. Mouse genome database (mgd) 2019. *Nucleic acids research*, 47(D1):D801–D806, 2019.
- James M Cheverud. A simple correction for multiple comparisons in interval mapping genome scans. *Heredity*, 87(1):52–58, 2001.
- James F Crow and Motoo Kimura. *An introduction to population genetics theory*. Harper & Row, 1970.
- Lien Dejager, Claude Libert, and Xavier Montagutelli. Thirty years of mus spretus: a promising future. *Trends in Genetics*, 25(5):234–241, 2009.
- RW Doerge, ZB Zeng, and BS Weir. Statistical issues in the search for genes affecting quantitative traits in experimental populations. *Statistical Science*, pages 195–219, 1997.
- Janis S Fisler, Craig H Warden, Mario J Pace, and Aldons J Lusis. Bsb: a new mouse model of multigenic obesity. *Obesity research*, 1(4):271–280, 1993.
- Nicholas W Galwey. A new measure of the effective number of tests, a practical tool for comparing families of non-independent significance tests. *Genetic Epidemiology*, 33(7):559–568, 2009.
- Yehudit Hasin, Marcus Seldin, and Aldons Lusis. Multi-omics approaches to disease. *Genome biology*, 18(1):1–15, 2017.
- James M Heather and Benjamin Chain. The sequence of sequencers: The history of sequencing dna. *Genomics*, 107(1):1–8, 2016.
- WG Hill and Alan Robertson. Linkage disequilibrium in finite populations. *Theoretical and applied genetics*, 38(6):226–231, 1968.
- JAX. JAX Stock #000664. Technical report, The Jackson Laboratory, 2022. URL <https://www.jax.org/strain/000664>.
- Daniel C Koboldt, Karyn Meltz Steinberg, David E Larson, Richard K Wilson, and Elaine R Mardis. The next-generation sequencing revolution and its impact on genomics. *Cell*, 155(1):27–38, 2013.
- DD Kosambi. The estimation of map distance from recombination values. *Annals of Eugenics*, 12(1):172–175, 1943.
- Thomas LaFramboise. Single nucleotide polymorphism arrays: a decade of biological, computational and technological advances. *Nucleic acids research*, 37(13):4181–4193, 2009.
- Eric S Lander and David Botstein. Mapping mendelian factors underlying quantitative traits using RFLP linkage maps. *Genetics*, 121(1):185–199, 1989.
- J Li and L Ji. Adjusting multiple testing in multilocus analyses using the eigenvalues of a correlation matrix. *Heredity*, 95(3):221–227, 2005.
- Ben Hui Liu. *Statistical genomics: linkage, mapping, and QTL analysis*. CRC press, 1998.

- NCBI. NCBI dbSNP Build 155, 2021. URL https://www.ncbi.nlm.nih.gov/projects/SNP/snp_summary.cgi.
- Dale R Nyholt. A simple correction for multiple testing for single-nucleotide polymorphisms in linkage disequilibrium with each other. *The American Journal of Human Genetics*, 74(4):765–769, 2004.
- LB Rowe, JH Nadeau, R Turner, WN Frankel, VA Letts, JT Eppig, MSH Ko, SJ Thurston, and EH Birkenmeier. Maps from two interspecific backcross dna panels available as a community genetic mapping resource. *Mammalian Genome*, 5(5):253–274, 1994.
- Daria Salyakina, Shaun R Seaman, Brian L Browning, Frank Dudbridge, and Bertram Müller-Myhsok. Evaluation of Nyholt’s procedure for multiple testing correction. *Human heredity*, 60(1):19–25, 2005.
- David Siegmund and Benjamin Yakir. *The statistics of gene mapping*. Springer Science & Business Media, 2007.
- Vivian Tam, Nikunj Patel, Michelle Turcotte, Yohan Bossé, Guillaume Paré, and David Meyre. Benefits and limitations of genome-wide association studies. *Nature Reviews Genetics*, 20(8):467–484, 2019.
- Emil Uffelmann, Qin Qin Huang, Nchangwi Syntia Munung, Jantina de Vries, Yukinori Okada, Alicia R Martin, Hilary C Martin, Tuuli Lappalainen, and Danielle Posthuma. Genome-wide association studies. *Nature Reviews Methods Primers*, 1(1):1–21, 2021.
- Peter M Visscher and Michael E Goddard. From RA Fisher’s 1918 paper to GWAS a century later. *Genetics*, 211(4):1125–1130, 2019.
- Carrie L Welch, Yu-Rong Xia, Ishaiahu Shechter, Robert Farese, Margarete Mehrabian, Shahab Mehdizadeh, Craig H Warden, and Aldons J Lusis. Genetic regulation of cholesterol homeostasis: chromosomal organization of candidate genes. *Journal of Lipid Research*, 37(7):1406–1421, 1996.
- Shizhong Xu. *Principles of statistical genomics*, volume 571. Springer, 2013.